Committee 5
Non-linear Structures in Natural Science and Economics

Draft – February 1, 2000
For Conference Distribution Only

Patterns, Waves, and Solitons in Fluids

Manuel G. Velarde
Professor of Physics
Universidad Complutense
Instituto Pluridisciplinar
Madrid, Spain

The Twenty-second International Conference on the Unity of the Sciences
Seoul, Korea February 9-13, 2000

SYMPOSIUM (CHAIRMAN: PROF. A. KINGSEP) NONLINEAR STRUCTURES IN NATURAL SCIENCES AND ECONOMICS

PATTERNS, WAVES AND SOLITONS IN FLUIDS

MANUEL G. VELARDE
Instituto Pluridisciplinar
Paseo Juan XXIII, 1
28040-Madrid, (Spain)

FAX (34) 91-394 32 43
Phone (34) 91-394 3242

ABSTRACT

When energy is supplied to a (nonlinear) dissipative system the possibility exists of exciting patterns or modes of self-organization that break the initial symmetry (or homogeneity) of the system. In the case of fluids this possibility is always a consequence of an instability of a given (diffusive) motionless state or flow field. Here, for illustration, follows a review of recent theoretical, numerical and experimental work on the creation of steady (and time-varying) cellular interfacial convective structures, the evolution from one to another of such patterns and how defects spontaneously evolve in time, for a given value of the external constraint. Results are also given about the excitation of (nonlinear) interfacial dissipative waves and (dissipative) solitons or shocks (hydraulic jumps, kinks or bore-like structures) as a generalization to dissipative flows of the classical work (Korteweg-de Vries-Boussinesq) on conservative systems. Data is also provided on their common (kinematic) properties in collisions and reflections at walls. Bound states and space chaotic states are also possible solitonic structures. Most of the results here reported have dynamical properties of expected universal value and hence may be shared by phenomena in other realms of science (chemistry, elasticity, neurobiology, chemical engineering, etc).

1 PATTERNS AND THEIR EVOLUTION NEAR A THERMOCONVECTIVE INSTABILITY THRESHOLD

The onset of patterned convective motions in heated fluid layers with a free upper surface has been extensively studied since the seminal experiments by Bénard (Bénard, 1900; Bénard, 1901; Koschmieder, 1993; Normand et al., 1977; Velarde and Normand, 1980). Depending on the depth of the layer, d, one distinguishes two basic mechanisms of instability. In sufficiently deep layers or in containers where the fluid is confined between rigid horizontal plates, the convective motion settles when buoyancy forces overcome viscous forces and heat dissipation (Rayleigh–Bénard problem). Alternatively, under microgravity conditions or in shallow enough layers with an open surface, inhomogeneity in the surface-tension, hence the Marangoni effect

is responsible for the onset of motion (Bénard–Marangoni problem). In both cases, the characteristic wavelength of the convective structure is about the depth of the cell or much larger, depending on whether or not the horizontal boundaries are good thermal conductors. Close to the instability threshold the system may be described by amplitude equations whose coefficients depend on the dimensionless numbers of the problem containing fluid properties, parameters of the boundary conditions and of the external forcing. One is the Biot number, $\mathrm{Bi} = hd/\kappa$, where h and κ are the heat transfer coefficient and the thermal conductivity of the liquid. Its infinite 'value' corresponds to a perfectly conducting boundary while a zero value is that of a poorly conducting surface.

In this Section we concentrate on the case where buoyancy is neglected but not gravity. Non-zero gravity, however small, rules out a spurious no-threshold convective flow at zero wave number. To the Navier–Stokes, continuity and energy equations, in the Boussinesq approximation (Normand et al., 1977; Pérez-Cordón and Velarde, 1975; Velarde and Pérez-Cordón, 1976; Ostrach, 1982; Davis, 1987), we add the boundary conditions. At the lower uniformly heated rigid plate, $v = 0$ and $\partial T/\partial z = \mathrm{Bi}\, T$. At the top open surface, $w = 0$, $\partial\sigma/\partial x = \eta\partial u/\partial z$, $\partial\sigma/\partial y = \eta\partial v/\partial z$ (Marangoni stresses), and $\partial T/\partial z = -\mathrm{Bi}\, T$; also, the Laplace boundary condition, with appropriate hydrostatic part for pressure, and the kinematic boundary condition for the transverse deformation of the surface hold. T, η, u and v, and w denote, respectively, temperature, dynamic viscosity, horizontal components of the velocity, and vertical component of the velocity. To study the transition between the motionless state and convection, and the dynamics of the structures that define this convective state, a multiple scale perturbation theory was developed in the vicinity of the onset of surface tension gradient-driven (Marangoni-driven) convection. Details can be found in (Bragard and Velarde, 1997 ; Bragard and Velarde, 1998) where reference is also given to related recent work by other authors. A small parameter allows separating the fast variables that describe the instability and the slow ones describing the pattern dynamics. For instance, the temperature can be written as:

$$\begin{aligned} T &= T(z)\Big[A_1(X,Y,\tau)\exp(i\underline{k}^{(1)}\cdot\underline{r}) + A_2(X,Y,\tau)\exp(i\underline{k}^{(2)}\cdot\underline{r}) \\ &\quad + A_3(X,Y,\tau)\exp(i\underline{k}^{(3)}\cdot\underline{r}) + \text{c.c.}\Big] \end{aligned}$$

where $\underline{k}^{(i)}$ denotes three linearly critical-wave vectors oriented at 120 degrees in the horizontal plane. The amplitude equations in the horizontal plane are (e.g. for A_1):

$$\begin{aligned} \alpha_t\partial_t A_1 &= \alpha_t\Delta A_1 + \alpha_q A_2^* A_3^* - \alpha_{cs}A_1|A_1|^2 - \alpha_{ci}A_1\left(|A_2|^2 + |A_3|^2\right) \\ &\quad + \alpha_d\left(\underline{k}^{(1)}\cdot\underline{\nabla}_x\right)^2 A_1 + i\beta_1\left(\underline{k}^{(1)}\cdot\underline{\nabla}_x\right)(A_2^* A_3^*) \\ &\quad + i\beta_2\left[A_2^*\left(\underline{k}^{(2)}\cdot\underline{\nabla}_x\right)A_3^* + A_3^*\left(\underline{k}^{(3)}\cdot\underline{\nabla}_x\right)A_2^*\right] \\ &\quad + i\beta_3\left[A_3^*\left(\underline{k}^{(2)}\cdot\underline{\nabla}_x\right)A_2^* + A_2^*\left(\underline{k}^{(3)}\cdot\underline{\nabla}_x\right)A_3^*\right], \end{aligned}$$

where $\alpha_1 = 0.0038$, $\alpha_t = 0.05 + 0.013\,\mathrm{Pr}^{-1}$, $\alpha_q = 0.0203 - 0.0046\,\mathrm{Pr}^{-1}$, $\alpha_{cs} = 0.016 + 0.0049\,\mathrm{Pr}^{-1} + 0.00077\,\mathrm{Pr}^{-2}$, $\alpha_{ci} = 0.0217 + 0.003\,\mathrm{Pr}^{-1} + 0.0018\,\mathrm{Pr}^{-2}$, $\alpha_d = 0.0021$, $\beta_1 = \beta_2 = \beta_3 = \beta = 0.0016 - 0.0041\,\mathrm{Pr}^{-1}$, and $\Delta = M - M_c$. $\mathrm{Pr} = \nu/\chi$ is the Prandtl number and $M = -\sigma_T\Delta T d/\eta\chi$ is the Marangoni number. ΔT denotes the (transverse) temperature difference across the liquid layer depth d. $\sigma_T = d\sigma/dT < 0$, for standard liquids. ν and χ are

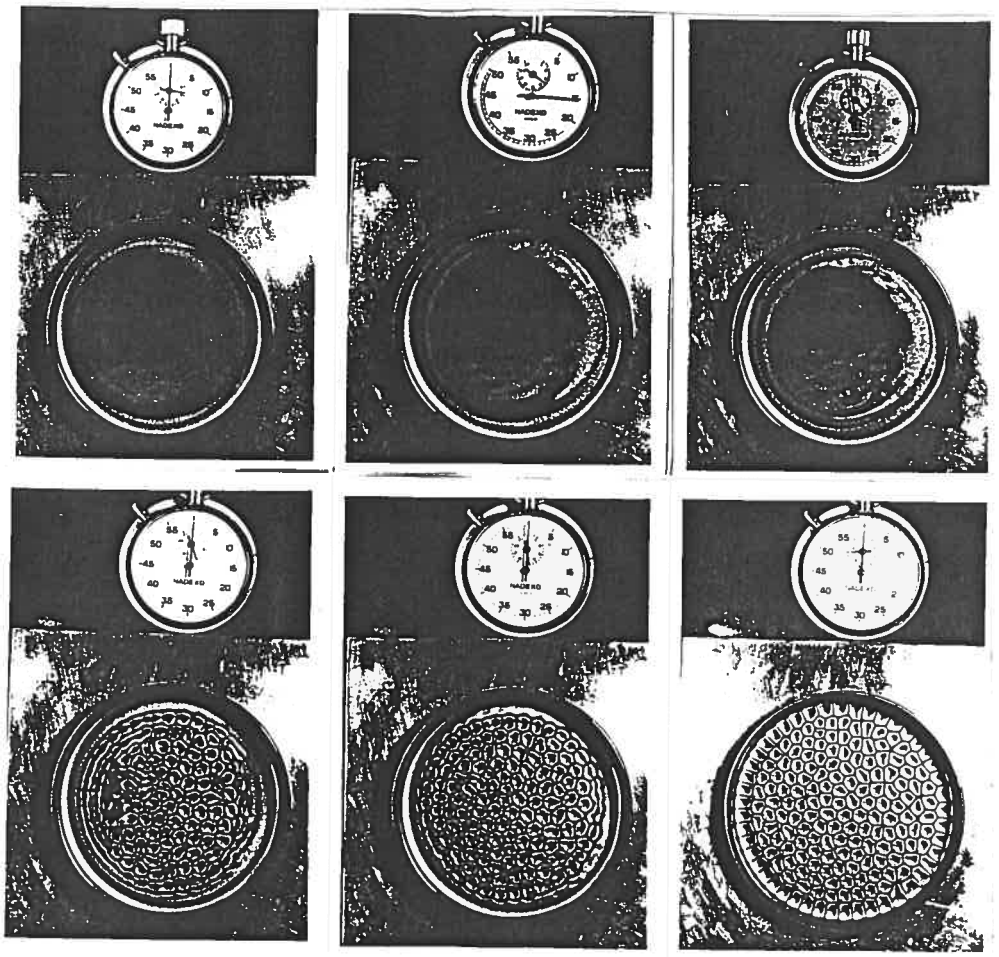

Fig. 1. The onset of BENARD cells in a shallow silicone oil layer (mm size)heated from below (the solid support made of copper) and open to ambient air.

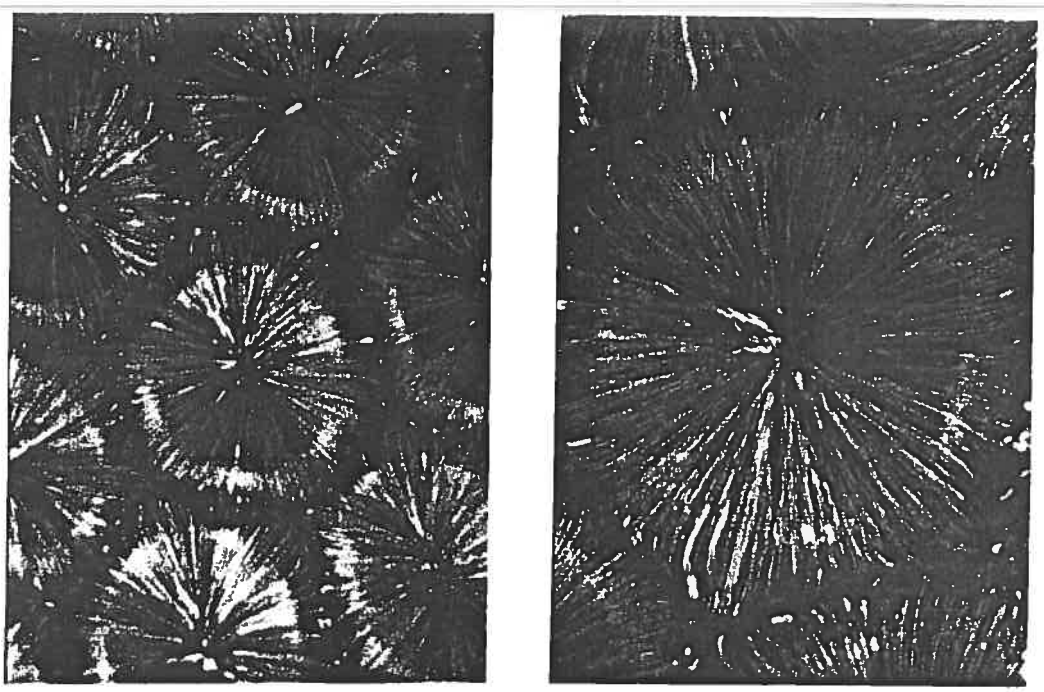

Fig. 2 Close-up of BENARD cells (hexagons) and streamlines with long exposure time.

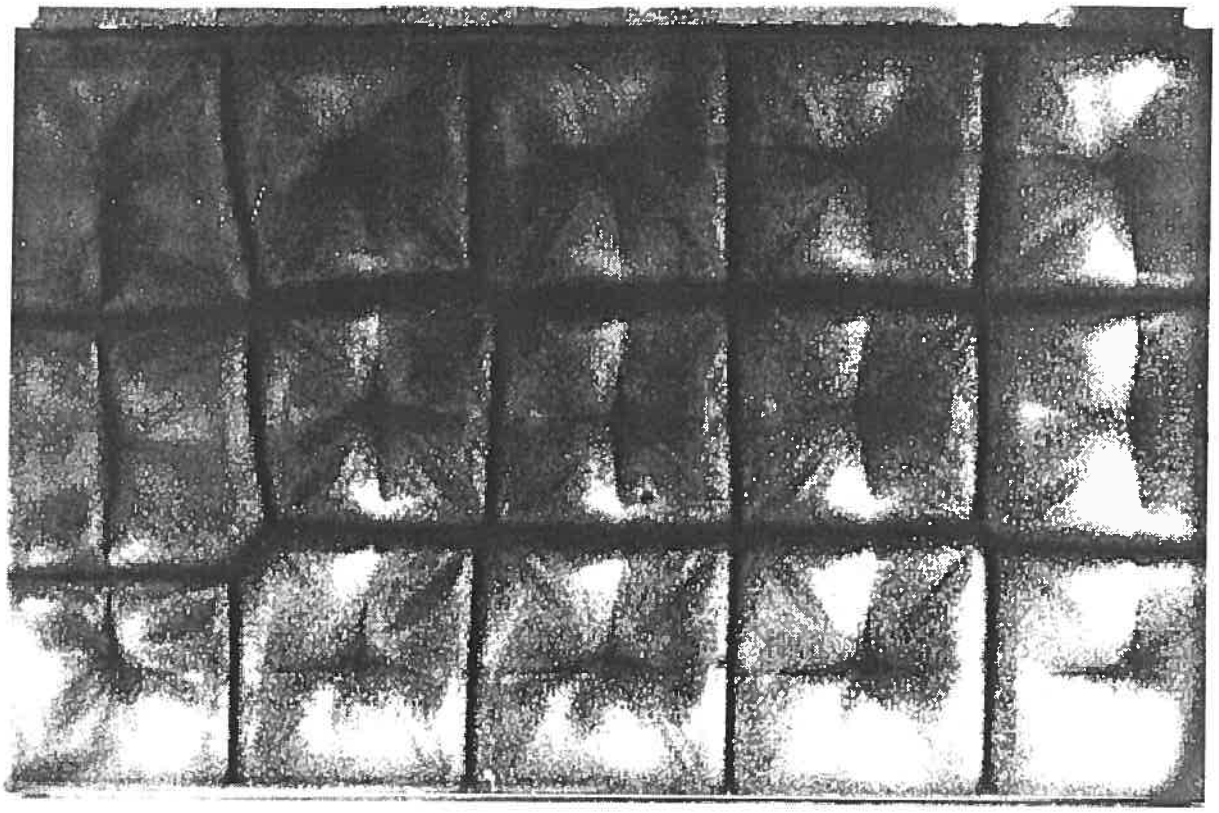

Fig. 3 BENARD cells in the form of square pattern

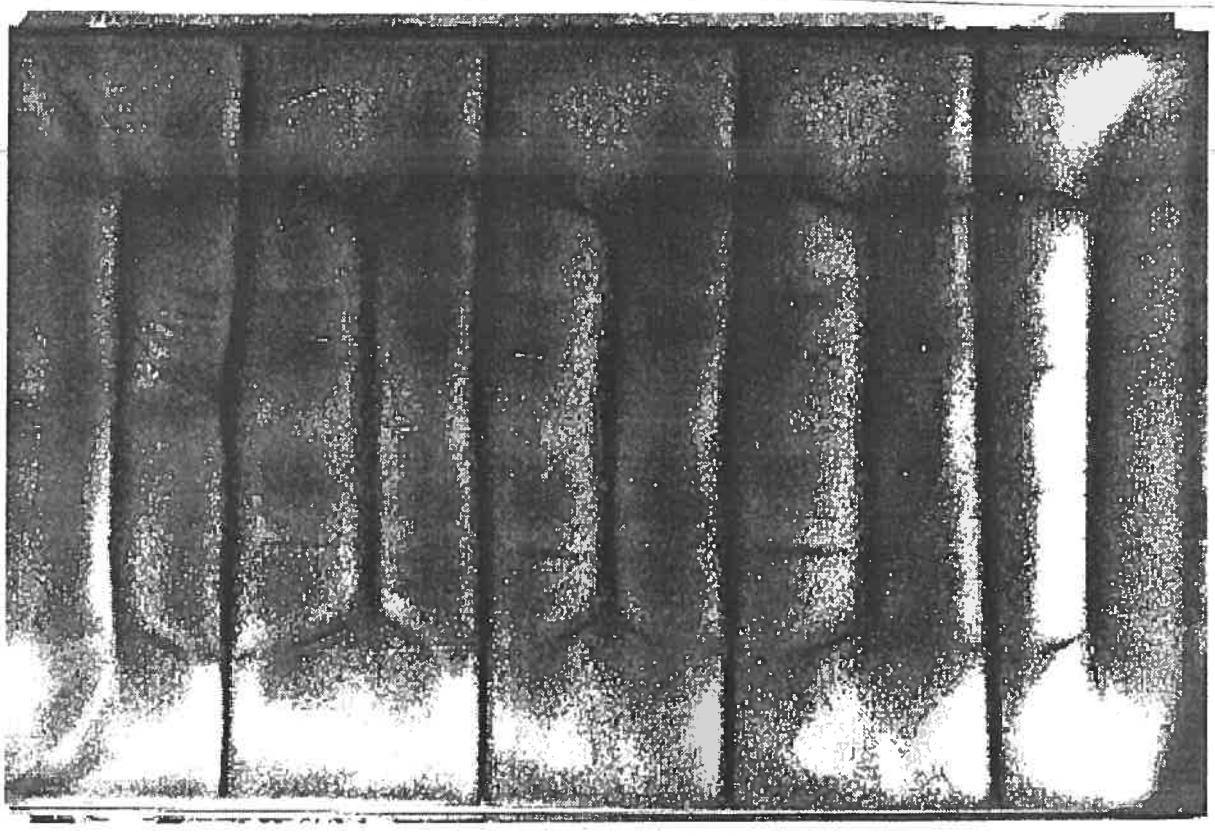

Fig. 4 BENARD cells in the form of roll-pattern

kinematic viscosity and thermal diffusivity, respectively $\eta = \nu\rho$, with ρ the liquid density. Similar equations appear for A_2 and A_3 (with circular permutation of the indices). The numbers correspond to the specific case of a poor conducting upper surface and good conducting lower plate as in standard experiments. These equations are generalized Ginzburg–Landau equations with advective terms with nonvanishing β coefficients. In general, for these equations there is no Lyapunov functional hence for some value of the βs we may observe no steady behavior. Δ and β measure the (sub/supercritical) distance to the threshold and the strength of the advective terms, respectively. In the simpler case of $\mathrm{Pr} \to \infty$ we define

$$\begin{aligned}
\Delta_c &= -\frac{\alpha_q^2}{4\alpha_1(\alpha_{cs}+2\alpha_{ci})} \approx -0.456\,, \\
\Delta_1 &= -\frac{\alpha_q^2\alpha_{cs}}{\alpha_1(\alpha_{cs}-\alpha_{ci})^2} \approx -53.4\,, \\
\Delta_2 &= -\frac{\alpha_q^2(2\alpha_{cs}+\alpha_{ci})}{\alpha_1(\alpha_{cs}-\alpha_{ci})^2} \approx 179.2\,.
\end{aligned}$$

Computations and stability analysis show two hysteresis cycles, hence coexistence and bistability appears in the intervals $[\Delta_c, 0]$ and $[\Delta_1, \Delta_2]$, respectively.

As an illustration, for a square container starting from random initial conditions (cases i-iv) or rolls (v) here are some results:

i. ($\Delta = 50$, $\beta = 0.1$). The system evolves to a stationary hexagonal pattern (Bénard cells). Relative to the case $\beta = 0$ an increase of β only slightly distorts the pattern. The fluid rises in the center of the cells in accordance with experimental observations. No defects are observed.

ii. ($\Delta = 75$, $\beta = 0$). The system is in a bistable region of hexagons and rolls.

iii. ($\Delta = 150$, $\beta = 0$). The rolls are the preferred structure. At boundaries, the rolls tend to be perpendicular to the sidewalls.

iv. ($\Delta = 150$, $\beta = 0.1$). The system does not reach a steady state. On the background of the roll structure, defects appear moving through the system.

v. ($\Delta = 150$, $\beta = 0.1$). Here the computation is with the same parameter values as in iv but with rolls plus noise added as initial condition. First, the structure evolves to rolls without defects, but as time goes on the rolls start to bend leading to a 'zig-zag'-like instability (Busse, 1978). The system does not show evolution to a steady state. It rather tends to a labyrinthine structure and possibly interfacial "turbulence," a form of spatio-temporal chaos or dissipative turbulence at variance with the (mostly) inertial turbulence of Reynolds and Kolmogorov (Batchelor, 1953 ; Frisch, 1995 ; Manneville, 1990). Another striking result is the (periodic) oscillatory alternance of hexagons and rolls in the absence of buoyancy (Bragard and Velarde, 1997 ; Bragard and Velarde, 1998).

2 INTERFACIAL WAVES AND SOLITONS: SCALING AND HEURISTIC ARGUMENTS

Let us consider now the liquid layer of depth d heated from the air side or open to suitable mass adsorption of a "light" component from a vapor phase above, with subsequent absorption in the bulk hence creating a (stabilizing) thermal gradient inside the liquid layer. Contrary to

the case of a layer heated from the liquid side, here we consider that, if buoyancy exists, the layer is stably stratified and hence oscillatory motions, waves, and not Bénard cells are to be observed (Levich, 1965; Sternling and Scriven, 1959; Edwards et al, 1991).

Generally, the problem with Marangoni stresses, gravity and buoyancy, involves several time scales. On the one hand we have the viscous and thermal scales, $t_{\rm vis} = d^2/\nu$, $t_{\rm th} = d^2/\chi$, respectively. There also exist two time scales associated with gravity and surface tension (Laplace overpressure) that tend to suppress surface deformation, $t_{\rm gr} = (d/g)^{1/2}$ and $t_{\rm cap} = (\rho d^3/\sigma)^{1/2}$. The time scale related to the Marangoni effect is $t_{\rm Mar} = (\rho d^2/|\sigma_T \beta|)^{1/2}$. Here $\beta = \Delta T/d$, and in this section $\beta > 0$ when heating from below. There is also another time scale related to buoyancy due to the stratification imposed by the temperature gradient, $t_{\rm st} = (1/|\alpha\beta|g)^{1/2}$. α is the thermal expansion coefficient, positive for standard liquids. As in the preceding Section the ratios of the time scales give rise to dimensionless groups ${\rm Pr} = t_{\rm th}/t_{\rm vis} = \nu/\chi$, $M = t_{\rm th}t_{\rm vis}/t_{\rm Mar}^2 = -\sigma_T \beta d^2/\eta\chi$, $R = t_{\rm th}t_{\rm vis}/t_{\rm st}^2 = \alpha\beta g d^4/\nu\chi$, $G = t_{\rm th}t_{\rm vis}/t_{\rm gr}^2 = g d^3/\nu\chi$, $B = t_{\rm cap}^2/t_{\rm gr}^2 = \rho g d^2/\sigma$, which are the already defined Prandtl and Marangoni numbers and the Rayleigh, Galileo and (static) Bond numbers, respectively.

These time scales are not always of the same order of magnitude. For example, for the simplified problem treated by Pearson (Pearson, 1958) when dealing with the onset of Bénard cells as the consequence of a Marangoni-driven instability in a liquid layer with undeformable surface, $M \approx 1$, but $G \gg 1$ and $R \ll M$. Indeed, although Pearson neglected gravity his assumption of undeformability was practically equivalent to gravity being able to keep the surface level, whatever flows and thermal inhomogeneities exist. He also neglected buoyancy in the bulk. The characteristic time scale of the problem is $t_{\rm th} \approx t_{\rm vis} \approx t_{\rm Mar}$ (at ${\rm Pr} \approx 1$). For monotonic instability hence the case leading to Bénard cells when heating the liquid layer from the liquid side there exists a finite limit of the critical Marangoni number as $G \to \infty$. As oscillatory instability does not appear in the one layer problem with undeformable surface. We expect that if such instability is possible the critical Marangoni number diverges with $G \to \infty$. Thus the critical Marangoni number should better be scaled with G, as G becomes very large ($G \to \infty$) in agreement with earlier studies (Chu and Velarde, 1988 ; García-Ybarra and Velarde, 1987).

We see clearly how a microgravity or variable-g experiment would allow to see the instability and the enhancement of the waves. In the very simplified case-studied by Garcia-Ybarra and Velarde (1987), the theoretical result predicted a universal relationship between temperature gradient and gravity $\beta \sim g^{5/8}$ as g is reduced, and hence a drastic lowering of the threshold as the effective gravity goes down, a striking result, indeed.

For high enough values of G an oscillatory mode is the capillary-gravity wave. The time scales $t_{\rm gr}$ and $t_{\rm cap}$ associated with this two-fold wave are much smaller than the viscous and thermal time scales (at least for ${\rm Pr} \approx 1$, $B \approx 1$). Then dissipative effects are relatively weak and the dispersion relation is $\omega^2 = G\,{\rm Pr}\,k(1 + k^2/B)\tanh(k)$ (to nondimensionalize ω the thermal time scale is used hereafter, k is the dimensionless wave number in units of d^{-1}). Clearly, the higher is G (and the wave frequency), the stronger should be the work of the Marangoni stresses (i.e. the higher is critical Marangoni number) to excite and sustain capillary-gravity waves. For a standard liquid, $\sigma_T < 0$, this instability appears when heating the liquid layer from the air side ($M < 0$), as expected.

The capillary-gravity wave is not the only possible wave motion in the liquid layer. When, the Marangoni number is high enough (and negative), there also exists another high-frequency

oscillatory mode. Indeed, when a liquid element rises to the surface, it creates a cold spot there. Then, the surface tension gradient acts towards this spot, pushing the element back to the bulk, and hence overstability. High values of M ensure that the oscillations exist. Let their characteristic time scale be also t_{Mar}. The corresponding wave is called "longitudinal", dilational or viscous as it is due to the Marangoni stresses along the surface in contrast to capillary-gravity waves with essentially transverse motion of the surface (Lamb, 1945 ; Lucassen, 1968). Calculation yields the following expression for the frequency of the longitudinal wave (in the limit $M \to -\infty$), $\omega^2 = -M[\mathrm{Pr}/(\mathrm{Pr}^{1/2}+1)]k^2$. Although this longitudinal wave has a genuinely dissipative nature, the damping rate is asymptotically smaller, $\mathcal{O}(|M|^{1/4})$, than its frequency. Up to some extent the flow field accompanying the dilational wave is qualitatively similar to that of the capillary-gravity wave. Potential flow can be assumed in the bulk of the layer, while vorticity is present only in boundary layers at the bottom rigid plate and at the upper free surface. The boundary layer thickness is of order of $\mathcal{O}(|M|^{-1/4})$ $[\mathcal{O}(G^{-1/4})]$. For the longitudinal wave the horizontal velocity field in the surface boundary layer is stronger than the potential flow in the bulk (by $\mathcal{O}(|M|^{1/4})$) at variance with the capillary-gravity wave. Thus, the longitudinal motion is really concentrated near the surface. Furthermore, it appears that with an undeformable surface ($1 \ll |M| \ll G$), the longitudinal mode is always damped. Indeed, as already said oscillatory instability does not appear in the one layer (Bénard-Marangoni) problem without surface deformability. However, if the longitudinal wave is accompanied by non-negligible surface deformation ($|M| \geq G$), it can be amplified, another striking result. Clearly, we see again the relevance of the microgravity experiment.

Thus, at $G \gg 1$, two thresholds for oscillatory Marangoni instability are expected with corresponding two (high-frequency) wave modes, capillary-gravity and longitudinal, dilational or viscous wave motions. As already said, to sustain the longitudinal wave one needs surface deformability. Alternatively, to sustain a capillary-gravity wave one needs the Marangoni effect. This is the tight coupling between capillary-gravity and longitudinal waves if they are to appear and be sustained past an instability threshold. The most dramatic manifestation of this coupling occurs at resonance, when the corresponding, generally different, frequencies are equal to each other. Near resonance there is mode-mixing. Namely, the capillary-gravity mode in the parameter half-space from one side of the resonance manifold is swiftly converted into the longitudinal one when crossing the manifold, and vice-versa. Another feature of resonance is that the damping/amplification rates are drastically enhanced here, namely, $\mathcal{O}(G^{3/5})$ versus $\mathcal{O}(G^{1/4})$ far from resonance.

If the liquid layer is deep enough and has an undeformable surface the possibility also exists of coupling dilational waves to internal (negative buoyancy-driven) waves with $|R| \ll G$. This may be called the Rayleigh–Marangoni problem. The role of the capillary-gravity wave is now played by the Brunt-Väisälä frequency $\omega^2 = -R\,\mathrm{Pr}[k^2/(k^2+n^2\pi^2)]$, $(n = 1, 2, \ldots)$, for a stably stratified layer when heating it from above. Note, that again lowering the effective gravity level this wave fades away as the stratification disappears. The wave-wave coupling is now between internal and longitudinal waves. In the absence of the Marangoni effect, no oscillatory motion via instability is possible, which again stresses the crucial role played by the coupling of the two wave disturbances.

Although general features of mode coupling are similar in the two problems, there are differences. In the Rayleigh-Marangoni case we have a countable number $(n = 1, 2, \ldots)$ of internal wave modes, and the longitudinal wave can be coupled to each of them, and hence

we have a countable number of marginal stability conditions. The form of the marginal curves is qualitatively different. Furthermore, there exists the minimally possible Rayleigh number (in absolute value), below which there is no oscillatory instability. No such bound was found for the Galileo number in the first problem (at least in the region where G remains high). A thoroughly detailed study of all these overstable motions and their corresponding mode-mixing can be found in (Rednikov at al., 1998; Rednikov at al., 2000).

3 NONLINEAR WAVES: ASYMPTOTIC EQUATIONS

The nonlinear evolution past threshold of either capillary-gravity or dilational waves poses formidable tasks. Let us then concentrate, for one of the two possible waves, on a simplified analysis although amenable to experimental test, and let us note the relevance of microgravity. We already said that the lower the gravity level the easier to excite those waves. Consider the horizontal liquid layer open to air and heated from above where "long" (a term to be made precise later on) capillary-gravity waves can be excited. As earlier, the liquid layer is placed on a flat rigid support but now the air layer is bounded from above by a flat rigid top which fits well with experimental set-ups. For simplicity, we assume that the layers are of infinite horizontal extent in one direction and treat the problem in two-dimensional geometry. A rest, there exists a linear vertical temperature distribution.

Let h_j here denote vertical depth and ρ_j density, ν_j kinematic viscosity, χ_j thermal diffusivity and κ_j thermal conductivity, where the subscripts $j = 1, 2$ refer to the liquid and gas layers, respectively. The corresponding symbols without subscript denote ratios: $\rho \equiv \rho_2/\rho_1$, $h = h_2/h_1$, $\nu \equiv \nu_2/\nu_1$, $\chi \equiv \chi_2/\chi_1$, and $\kappa \equiv \kappa_2/\kappa_1$. We assume that h is of order unity, while ν and χ are large enough, and ρ and κ are smaller than unity, in accordance with standard gas and liquid properties. The ratio of the dynamic viscosities, $\rho\nu$, is also small enough. The Prandtl number for both the liquid, $\mathrm{Pr} \equiv \nu_1/\chi_1$, and the gas, $P = \nu_2/\chi_2$, are also taken of order unity.

As we shall only consider "long" enough waves let us define a smallness parameter, ϵ, as the ratio of the depth to a characteristic wavelength. Then, there are two time scales in the problem. One of them is defined by heat diffusion, $t_{\mathrm{th}} = h_1^2/\chi_1$ (as Pr is assumed of order unity, the viscous time scale, $t_{\mathrm{vis}} = h_1^2/\nu_1$ is of order of the thermal one). The other time scale, $t_{\mathrm{gr}} = \epsilon(h_1/g^{1/2})$ is associated with "long" gravity waves, as g is the gravity acceleration; $\epsilon = G^{-1/10}$ is defined below. When $t_{\mathrm{th}} \ll t_{\mathrm{gr}}$ the heat and viscous effects are predominant which, in practice, corresponds to very shallow liquid layers or microgravity conditions. In the opposite situation, $t_{\mathrm{th}} \gg t_{\mathrm{gr}}$, the dissipation is limited to the boundary layers at the bottom and, if the Marangoni effect is significant, near the upper surface. In terms of the Galileo number the first case corresponds to $G\epsilon^2 \ll 1$, while in the second to $G\epsilon^2 \gg 1$. We shall all consider $G \gg 1$. Lowering the value of g affects the phenomenon and hence its microgravity relevance.

The thickness d of the boundary layers can be estimated as follows. We have $t_{\mathrm{gr}} \approx t_{\mathrm{th}}$ where t_{gr} is as earlier defined while for t_{th} we now have $t_{\mathrm{th}} = d^2/\chi_1$. Then we get

$$\frac{d}{h_1} \approx \frac{1}{\epsilon^{1/2} G^{1/4}} \,. \tag{1}$$

This shows that the boundary layer thickness diverges with $G^{-1/4}$. Once more we define dimensionless quantities using suitable scales: h_1 for length, $(gh_1)^{1/2}$ for velocity, $(h_1/g)^{1/2}$ for time, $\rho_1 g h_1$ for pressure in the liquid, $\rho_2 g h_1$ for pressure in the air, βh_1 for temperature in the liquid, $\kappa^{-1}\beta h_1$ for temperature in the air, where β is again the vertical temperature gradient in the liquid layer but with a change of sign in the convention taken here: now $\beta > 0$ corresponds to heating from above and $\beta < 0$ if heating is from below. By pressure and temperature we denote deviations of the corresponding quantities from their stationary distribution, linear with the vertical coordinate.

Let x and z be here the horizontal and vertical coordinates, respectively. The bottom of the layer is taken at $z = -1$, the free surface at $z = \eta(x,t)$, and the top of the air layer at $z = h$, where t is time and $\eta(x,t)$ describes the surface deformation. Thus as already mentioned we restrict consideration to 2D flow motions. Note that hereafter η does not refer to (dynamic) viscosity. To search for only "long" traveling wave motions in a shallow layer we redefine the horizontal variable, $\xi = \epsilon(x - Ct)$, where C is a phase velocity to be determined. In addition we scale horizontal velocity, pressure and deformation of the surface η with ϵ^2, vertical velocity with ϵ^3 and introduce the slow time scale $\tau = \epsilon^3 t$. The scale for temperature is determined by the leading convective contribution to the temperature field which is of order ϵ^2. Accordingly, the equations governing "long" wave disturbances are

$$u\xi + w_z = 0\,, \tag{2}$$

$$\epsilon^2 u_\tau - C u_\xi + \epsilon^2 w u_z = -p_\xi + \epsilon^{-1}\left(\frac{\mathrm{Pr}}{G}\right)^{1/2}\left(\epsilon^2 u_{\xi\xi} + u_{zz}\right), \tag{3}$$

$$\epsilon^4 w_\tau - \epsilon^2 C w_\xi + \epsilon^4 u w_\xi + \epsilon^4 w w_z = -p_z + \epsilon\left(\frac{\mathrm{Pr}}{G}\right)^{1/2}\left(\epsilon^2 w_{\xi\xi} + w_{zz}\right), \tag{4}$$

$$\epsilon^2 T_\tau - C T_\xi + \epsilon^2 u T_\xi + \epsilon^2 w T_z + w = \epsilon^{-1}\frac{1}{(\mathrm{Pr}\,G)^{1/2}}\left\{\epsilon^2 T_{\xi\xi} + T_{zz}\right), \tag{5}$$

$$U_\xi + W_z = 0\,, \tag{6}$$

$$\epsilon^2 U_\tau - C U_\xi + \epsilon^2 U U_\xi + \epsilon^2 W U_z = -\Pi_\xi + \epsilon^{-1}\left(\frac{\mathrm{Pr}}{G}\right)^{1/2}\nu\left\{\epsilon^2 U_{\xi\xi} + U_{zz}\right), \tag{7}$$

$$\epsilon^4 W_\tau - \epsilon^2 C W_\xi + \epsilon^4 U W_\xi + \epsilon^4 W W_z = -\Pi_z + \epsilon\left(\frac{\mathrm{Pr}}{G}\right)^{1/2}\nu\left(\epsilon^2 W_{\xi\xi} + W_{zz}\right), \tag{8}$$

$$\epsilon^2 \theta_\tau - C\theta_\xi + \epsilon^2 U\theta_\xi + \epsilon^2 W\theta_z + W = \epsilon^{-1}\left(\frac{\mathrm{Pr}}{G}\right)^{1/2}\frac{\nu}{P}\left(\epsilon^2\theta_{\xi\xi} + \theta_{zz}\right), \tag{9}$$

with the boundary conditions:
at $z = -1$:

$$u = w = T = 0\,, \tag{10}$$

at $z = h$:

$$U = W = \theta = 0\,, \tag{11}$$

and at $z = \eta(\xi,\tau)$:

$$w \;=\; \epsilon^2\eta_\tau - C\eta_\xi + \epsilon^2 u\eta_\xi = W\,, \tag{12}$$

$$u = U\,, \tag{13}$$

$$p = \eta - \epsilon^2\left[\frac{1}{B} - \epsilon^2\frac{M}{G}(T+\eta)\right]\frac{\eta_{\xi\xi}}{N^3} + \frac{2}{N^2}\epsilon\left(\frac{\mathrm{Pr}}{G}\right)^{1/2}\left[w_z - \epsilon^2\eta_\xi\left(u_z + \epsilon^2 w_\xi\right) + \epsilon^6 u_\xi\eta_\xi^2\right], \tag{14}$$

$$\left(u_z + \epsilon^2 w_\xi\right)\left(1-\epsilon^6\eta_\xi^2\right) + 2\epsilon^4\eta_\xi\left(w_x - u_\xi\right) + \frac{MN\epsilon}{(\mathrm{Pr}\,G)^{1/2}}\left(\eta_\xi + T_\xi + \epsilon^2\eta_\xi T_z\right) = 0\,, \tag{15}$$

$$\eta + \theta = 0\,, \tag{16}$$

$$T_z - \epsilon^4\eta_\xi T_\xi = \theta_z - \epsilon^4\eta_\xi\theta_\xi\,, \tag{17}$$

with

$$M \equiv -\frac{d\sigma}{dT}\frac{\beta h_1^2}{\rho_1\nu_1\chi_1}\,; \quad B \equiv \frac{\rho_1 g h_1^2}{\sigma}\,; \quad N \equiv \left(1+\epsilon^6\eta_\xi^2\right)^{1/2}.$$

We clearly see how the correction cannot be neglected when the effective gravity drastically goes down.

Note that we define M and B with the liquid layer properties. Here u, w, p and T denote the horizontal and vertical velocity components, pressure and temperature fields in the liquid layer. U, W, Π and θ denote the corresponding fields in the air layer. M and B correspond to the earlier defined (static) Bond numbers, respectively. B is assumed of order unity, while M is taken large enough as, indeed, the Marangoni effect is the control parameter leading to instability past a (high enough) threshold. The scaling of M with ϵ is provided when solving the problem. The dynamic properties of air are neglected in the normal (14) and tangential (15) stress balances. The smallness of κ permitted to write the boundary condition representing continuity of temperature across the surface, $T + \eta = \kappa^{-1}(\eta + \theta)$ in the form (16). Thus, κ as well as ρ disappear from the equations.

Now let us discuss what should be the relation between the smallness parameters ϵ and G^{-1} and hence the role of variable gravity. As long as we limit ourselves to the case $\epsilon^{-1/2}G^{-1/4} \ll 1$, i.e. to the case when the liquid layer can be subdivided into the bulk where the flow is potential and the boundary layers, the most interesting asymptotics corresponds to the case when the boundary layer thickness and the deformation of the surface are of the same order. From (1) follows that $\epsilon^{-1/2}G^{-1/4} \approx \epsilon^2$, i.e.

$$\epsilon = G^{-1/10}\,. \tag{18}$$

(We write "=" to define ϵ in terms of G). Then the effects of energy output (due to heat and viscous dissipation) and input (due to the Marangoni effect) will be of the same order as nonlinearity and dispersion. The latter two are in appropriate balance for the ideal liquid Korteweg-de Vries (KdV) equation for long waves in the shallow layer (Drazin and Johnson, 1989).

Turning to the equations in the air layer, we assume that due to its relatively large kinematic viscosity ($\nu \gg 1$) and thermal diffusivity ($\chi \gg 1$), inertia in the air is no more dominating over dissipative effects. Then in the most general case

$$a^2 \equiv \epsilon^{-1}\,\mathrm{Pr}^{1/2}\,G^{-1/2}\nu \approx 1\,.$$

The coefficients of the Laplacians in Eqs. (7,9) are a^2 and a^2/P, respectively. From (18), in the liquid layer, Eqs. (3,5), it follows that they are ϵ^4 and ϵ^4/Pr, respectively.

To solve the problem (2–17), all components of $f = (u, w, p, T, U, W, \Pi, \theta)$ are suitably expanded with ϵ.

For convenience we redefine the Marangoni number

$$m \equiv \frac{M\epsilon^{10}}{\mathrm{Pr}} = \frac{M}{G} \tag{19}$$

This modified Marangoni number, m, which is an inverse (dynamic) Bond number is of order unity and corresponds to the most general case as viscous and thermocapillary stresses are of the same order in the tangential stress balance. This also means that M is of order of G.

After long and cumbersome calculations, the following evolution equation for surface waves is obtained:

$$\begin{aligned} 2\left(1-\frac{m}{\mathrm{Pr}^{1/2}+1}\right)\left[\eta_\tau+\frac{3}{2}\eta\eta_\xi+\left(\frac{1}{6}-\frac{1}{2B}\right)\eta_{\xi\xi\xi}\right] \\ +\left(m\frac{2\,\mathrm{Pr}^{1/2}+1}{\mathrm{Pr}+\mathrm{Pr}^{1/2}}-1\right)\frac{1}{\pi^{1/2}}\frac{d}{d\xi}\int_\xi^\infty \frac{\eta(\xi')}{(\xi'-\xi)^{1/2}}d\xi' \\ +\frac{m}{\mathrm{Pr}^{1/2}}\frac{1}{\pi^{1/2}}\frac{d}{d\xi}\int_\xi^\infty \frac{Q(\xi')}{(\xi'-\xi)^{1/2}}d\xi' = 0\,. \end{aligned} \tag{20}$$

Eq. (20) is a dissipation-modified KdV equation describing "long" surface tension gradient-driven waves in a Bénard layer. It significantly generalizes earlier work (Chu and Velarde, 1999; Velarde et al., 1991; Garazo and Velarde, 1991; Nepomnyashchy and Velarde, 1994) and under appropriate limiting conditions reduces to the (ideal, standard) KdV equation. On the other hand another earlier dissipative KdV result with no Marangoni effect (Miles, 1976) follows from Eq.(20) by setting $m = 0$, as expected.

4 SOLITONS AS TRAVELING (LOCALIZED) DISSIPATIVE STRUCTURES: ENERGY BALANCE

The dissipation-modified KdV equation, (20), possesses the necessary ingredients to have solutions in the form of stationary propagating waves: there is an unstable wavenumber interval, where the energy is brought by the Marangoni effect and dissipation occurs on the wavenumbers belonging to the stability interval. The convective nonlinearity redistributes the energy from long to short waves, making possible the dynamic equilibrium and the appropriate energy balance for the dissipative wave. We may expect solutions such as sustained dissipative periodic wave trains or solitary waves as in earlier mentioned drastically simplified dissipation-modified KdV equations (Christov and Velarde, 1995; Nekorkin and Velarde, 1994; Velarde et al., 1995; Rednikov et al., 1995).

For the case of a thin air gap above the liquid layer ($h \ll 1$, however h should remain larger than the surface deformation). In this case, the air motion is dissipation-dominated. Then

$\theta = \eta(z-h)/h$, and $Q = \eta/h$. Using this in Eq.(20), we get

$$2\left(1-\frac{m}{\mathrm{Pr}^{1/2}+1}\right)\left[\eta_\tau + \frac{3}{2}\eta\eta_\xi\left(\frac{1}{6}-\frac{1}{2B}\right)+\eta_{\xi\xi\xi}\right]$$
$$+\left(m\frac{2\,\mathrm{Pr}^{1/2}+1}{\mathrm{Pr}+\mathrm{Pr}^{1/2}}+M\frac{1}{h\,\mathrm{Pr}^{1/2}}-1\right)\frac{1}{\pi^{1/2}}\frac{d}{d\xi}\int_\xi^\infty \frac{\eta(\xi')}{(\xi'-\xi)^{1/2}}d\xi' = 0. \qquad (21)$$

The critical (modified) Marangoni number is now

$$m_b = \left(\frac{2\,\mathrm{Pr}^{1/2}+1}{\mathrm{Pr}+\mathrm{Pr}^{1/2}}+\frac{1}{h\,\mathrm{Pr}^{1/2}}\right)^{-1}. \qquad (22)$$

An important fact is that m_b considerably decreases with decreasing h. Thus to observe sustained capillary-gravity waves as the result of Marangoni-driven instability, the thinner the air gap the better. Take, for example, a water-like liquid. For illustration choose $h_1 = 0.1$, $h_2 = 0.01$ ($h = 0.1$), $d\sigma/dT = -0.15$, $g = 10^3$ and $\mathrm{Pr} = 6$ (for dimensional quantities the CGS system is used). Then, according to Eq. (22), the temperature difference applied to the liquid layer needed to excite and sustain Marangoni-driven "long" capillary-gravity waves is 15 K, hence a 150 K/cm gradient. However, in the supercritical case, with Eq.(21) all wavenumbers are unstable. This is related to the fact that in the limit of high dissipation in the air layer ($h \ll 1$ or $a \gg 1$), the band of unstable wavenumbers shifts to higher and higher k, where our long wave approximation ceases to be valid. In this case, to obtain a suitable energy balance to maintain the waves we must proceed to a higher order approximation (ϵ^2 in Eq. (21)), hence $m - m_b \approx \epsilon^2$).

Finally, let us mention that the vanishing of the coefficient of the ideal KdV terms in Eq. (21), at $m = \mathrm{Pr}^{1/2}+1$, corresponds to the resonance between capillary-gravity and longitudinal waves. Our approach is not valid in the vicinity of this resonance point. However, note that the resonance value is always higher than m_b.

The energy balance just discussed greatly simplifies and becomes more transparent if we restrict consideration to the particular case of a stress-free boundary condition at the bottom of the liquid layer. This drastic simplification does not provide quantitative agreement with experiment but allows qualitative explanation of most of the phenomena found in experiment. In such a case Eq. (20) reduces to

$$\eta_\tau + (\eta^2)_y + \eta_{yyy} + \delta\left[\eta_{yy} + \eta_{yyy} + D\left(\eta^2\right)_{yy} + \alpha\eta\right] = 0\,, \qquad (23)$$

where $\eta(y,t)$ is a suitable scaled elevation of the surface for one-side, left-to-right steadily propagating waves. The coefficient D can be either positive or negative, while α and δ are nonnegative. When δ vanishes we indeed recover the KdV equation. For the extension of Eq. (23) to the cylindrical geometry see (Huang et al., 1998).

By multiplying Eq. (23) by η, and integrating over the full space or one wavelength the energy $E = \frac{1}{2}\int \eta^2 dx$ is governed by the balance

$$\frac{dE}{dt} = \delta\left(\int \eta_x^2\,dx - \int \eta_{xx}^2\,dx + 2D\int \eta\eta_x^2\,dx - \alpha\int \eta^2\,dx\right), \qquad (24)$$

whose value vanishes at the steady state. The first term on the right hand side of (23) describes the energy input at rather long wavelengths, due to instability, the second and fourth terms describe energy dissipation on short and long wave lengths, respectively, and the third term accounts for the convective nonlinearity redistributing energy as a (feedback) correction to long wave energy input (for η positive, positive if D is positive and negative otherwise). Recalling that the KdV equation possesses a one-parameter family of solitary waves or cnoidal waves (periodic wave trains) thanks to the dispersion-nonlinearity balance also existing in Eq. (23) we note that here the input-output energy balance (24) selects a single wave or a single amplitude periodic wave train, a bound state or an erratic/chaotic wave train.

On the other hand, when considering the three-dimensional problem as done by Nepomnyashchy and Velarde (1994), phase shifts following collision or reflection at walls depend upon the incident angle, α_i (e.g. measured front to front or twice the value front to wall, i.e. by $\pi/2 - \alpha_i$; a reflection is like a collision with a mirror image wave). At the approximate value of $\pi/2$ no phase shift is expected while for lower collision angles the phase shift has the sign of phase shifts upon head-on collisions. Higher values than $\pi/2$ (or $\alpha_i < \pi/4$) lead to a change of sign in the phase shift and the formation of a third wave evolving phase locked with the post collision or reflected front (hereafter called Mach-Russell stem). This result for Marangoni-driven waves generalizes a result obtained by Miles (Miles, 1977) for the dissipation-free (and $m = 0$) case. These (kinematic) phenomena were discovered a century ago by Russell (Russell, 1842) for water waves and by Mach (Krehl and van der Geest, 1991 ; Courant and Friedrichs, 1948) for shocks in gases. The phase-shift sign in such case is the same as the sign in the overtaking collisions discussed by Zabusky and Kruskal in their seminal paper where they introduced the soliton concept (Zabusky and Kruskal, 1965). Finally, starting with e.g. an initial condition of two nearby 'solitary' pulses the system evolves according to Eq. (23) to a bound state or wave train with unequally spaced crests or a form of chaotic still. All crests have the same value, hence the same velocity dictated by the energy balance (24) in the steady state, as numerically observed.

5 INTERFACIAL DISSIPATIVE SOLITARY WAVES AND SOLITONS: EXPERIMENTAL EVIDENCE

Both mass absorption and desorption, and heat transfer experiments have shown the onset and evolution of solitary waves, wavetrains and solitons. Research was carried out thirty years ago, nearly at the time when Zabusky and Kruskal caned the soliton concept, by H. Linde and collaborators in Berlin (for recent accounts see Refs. Weidman et al., 1992, Linde et al., 1993, Linde et al., 1993) and more recently in Madrid in collaboration with H. Linde (Linde et al., 1997; Wierschem et al., 1999; Linde et al., 2000). Related work has also recently been done by Santiago and Adler at CNRS, Meudon (Santiago-Rosanne, 1995 ; Santiago-Rosanne et al., 1997).

For the case of heat transfer (liquid depths from 0.3 to 0.8 cm) liquid octane was poured in square and cylindrical vessels, and in annular channels (1.5 and 2.0 cm inner and outer radii, respectively). The bottom was cooled by air or water at 20 C and the cover made of quartz placed at 0.3 cm above the liquid was heated hence establishing in the liquid layer a temperature gradient. For values of this gradient ranging from 10 to 200 K/cm (in the range predicted by

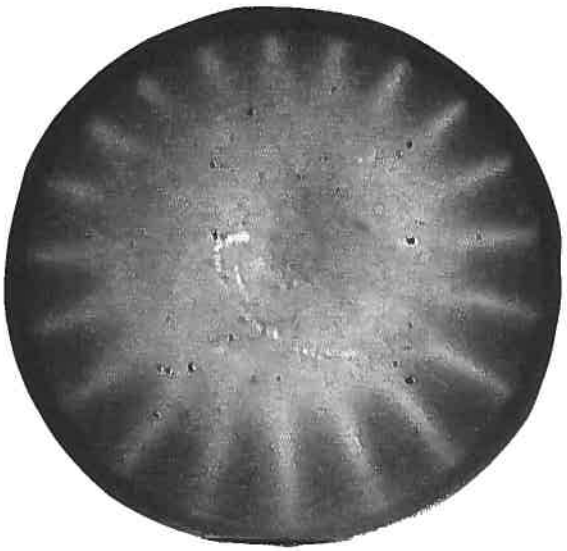

Fig. 5 Wavetrain formed in a shallow liquid layer heated from above (from the air side) or subjected to adsorption (and subsequent absorption) of a light surfactant (e.g. hexane on toulene).

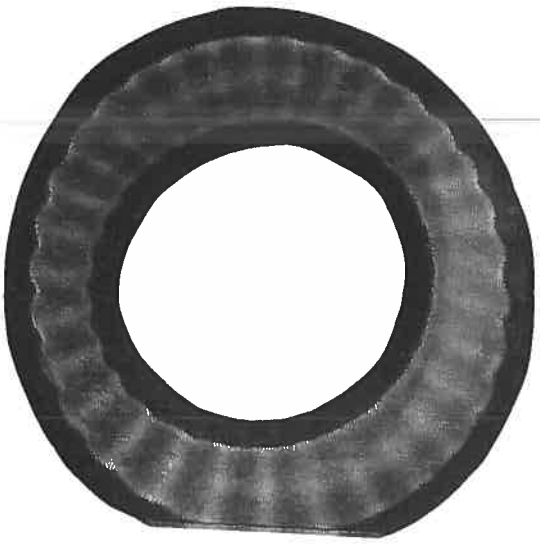

Fig. 6 Wavetrain as in Fig. 5 with a circular annular container.

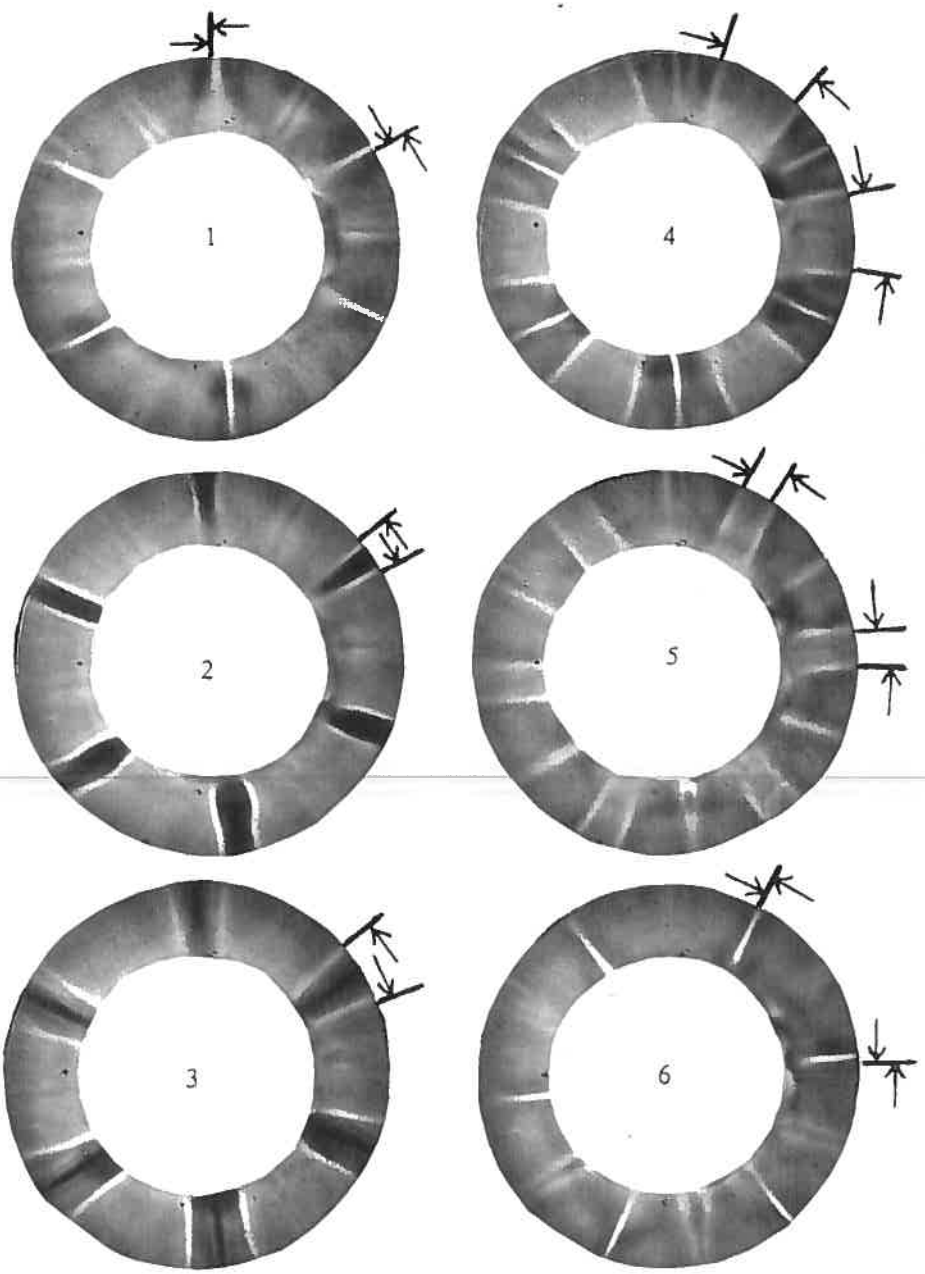

Fig. 7 Typical sequence of synchronic crest-collisions of two counterrotating wavetrains as described in Figs. 5 and 6. The events repeat for long time (in practical terms quarter of an hour to half hour)

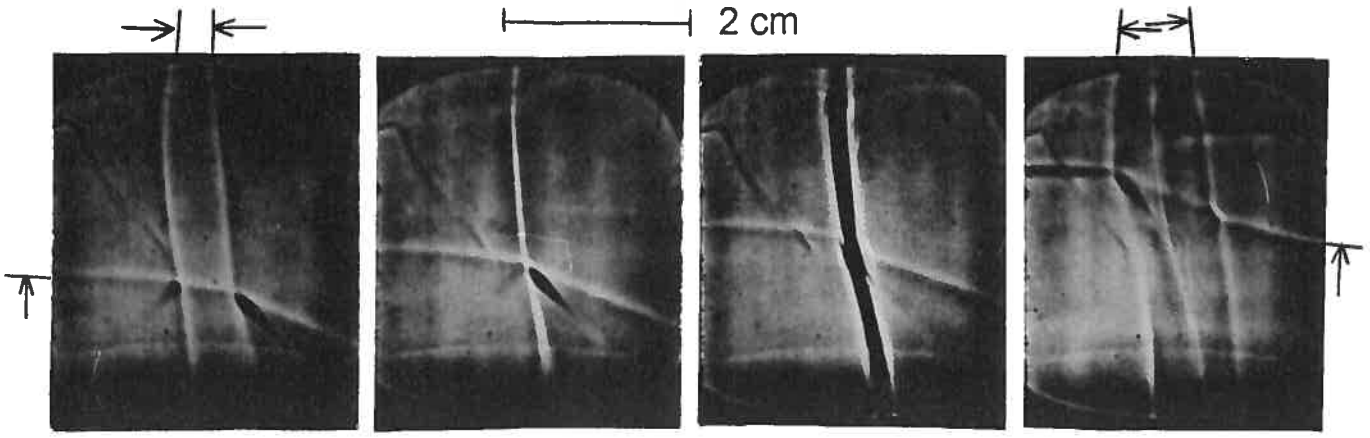

Fig. 8 Typical (solitary) waves colliding at various angles (with formation or not of the Mach-Russell thrid wave/stem). Liquid as in Figs. 5, 6 and 7.

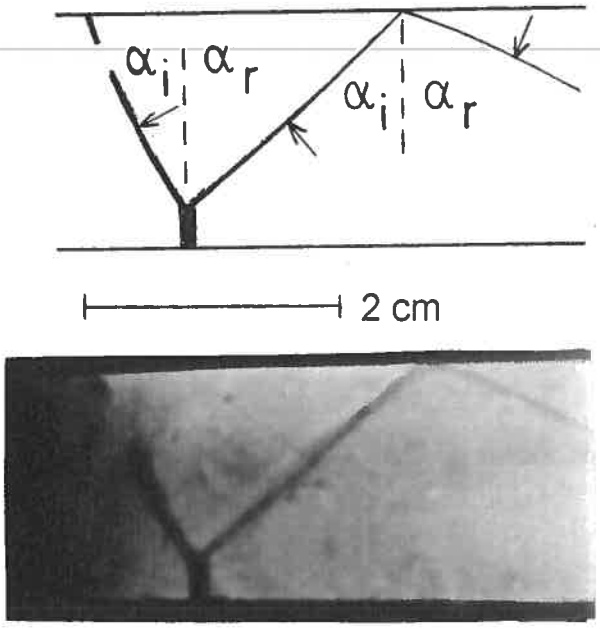

Fig. 9 Beautiful sequence of regular and Mach-Russell reflections at opposite walls. Liquid as in Figs. 5-8.

theory, as earlier described), solitary waves and periodic wave trains were observed showing properties similar to the waves also observed in mass transfer experiments.

For mass transfer the following set-up was used. A vessel A, either a cylindrical container or an annular channel, was filled with liquid (liquid depth 1.8 cm). Two surrounding vessels B_1 and B_2, clearly concentric with the annular chanel, were also filled with another liquid. With pentane in B_1 and B_2 either xylene, nonane, trichloroethylene or benzene were used as absorbing liquid in A, while with toluene as absorbing liquid in A either hexane, pentane, acetone or diethylether in B_1 and B_2 were used. In all cases the results were qualitatively the same. A glass cover, C, was placed on top of the vessels B_1 and B_2 and then when C was full of hexane vapor, say, it was placed on top of A thus allowing the absorption of hexane by the toluene liquid in A. The adsorption and subsequent absorption processes are rather strong, hence create Marangoni stresses high enough to trigger instability and sustain flow motions and, eventually, waves. During the whole duration of the experiment, hexane vapor was also allowed to diffuse from the two vessels B_1 and B_2 to A.

Observation and recording with a CCD camera was made by shadowgraph from the top with point-like illumination from the bottom up. For instance, with cylindrical or annular cylindrical containers, at first, rather violent chaotic motions occur along the surface in A with waves moving in practically all directions but finally after about one minute when most of the vapor in C has been absorbed, a dramatic self-organization leads to strikingly regular wave motion. Long time lasting, synchronically colliding counter-rotating periodic wave trains were observed in an annular channel for about 50 to 200 seconds while a single (periodic) wave train with either clockwise or counterclockwise rotation remained up to 450 seconds. When waves or counter-rotating wave trains collide typical mean wave velocities at the outer wall of the annular channel before and after collision were, respectively, 2.7 and 1.7 cm/s (corresponding to angular speeds of 71.4 degrees/s and 45.7 degrees/s, respectively). Thus the mean wave velocity right after collision was about 64% (with less than 2% error) the mean wave speed measured before collision. About 0.2 seconds after collision the original wave speed was recovered. Post-collision trajectories of solitary waves or wave crests experienced phase shifts like in the case of solitons (Darin and Johnson, 1989; Miles, 1977; Zabusky and Kruskal, 1965). Reflections at walls also illustrate the solitonic or shock behavior of the waves which occur with and without the formation of a (phase locked, third wave) Mach-Russell stem according to the angle of incidence (Russell, 1842; Krehl and van der Geest, 1991; Courant and Friedrichs, 1948). The experiments just described are unsteady, the phenomena observed are complex and, only recently, there have been clear-cut distinction between mostly surface waves and (mostly) internal waves (Rayleigh-Marangoni problem (Rednikov at al., 1997b), all of them triggered and sustained by the Marangoni effect. Further work remains to be done in this field.

6 Conclusion

Theoretical and experimental results have been provided to show how by means of an appropriate balance of energy (convective) patterns and nonlinear waves (and solitons) can be excited and sustained past an instability threshold. From *disorganized* motions (heat or mass diffusion) at and above threshold there appears organized cellular patterns or time-dependent motions (solitary waves, wavetrains of well defined period and amplitude, and solitons). The energy

input is crucial for otherwise if those (steady or traveling) dissipative structures were excited either spontaneously or by some instantaneous forcing they are bound to decay due to dissipation (heat, mass diffusion or viscous damping). Once there is continuous energy input structures can be maintained as long as we wish. Furthermore, with the energy balance operating the kind of structure that can be maintained depends on some other balance that we may add. For instance, for waves one such balance could be, in dynamic and hence evolving "equilibrium", nonlinearity and dispersion or between nonlinearity and diffraction (of great interest in light or wave transmission through optical fibers).

We have shown how solitons, soliton-bound states and even spatially chaotic soliton wavetrains can be excited and maintained in a dissipative system. We have also shown how, for a given value of the externally given energy input, as time proceeds we may have transitions from one pattern to another thus illustrating bistability in non-equilibrium dissipative systems.

The results presented here belong to fluid dynamics and, in particular, to interfacial phenomena. However, the basic arguments underlying the results presented have universal applicability well beyond fluid physics.

Acknowledgments

In the past years, we have benefited from the fruitful collaboration with Michèle Adler, J. Bragard, C. I. Christov, X.-L. Chu, P. Colinet, A. N. Garazo, G.-X. Huang, V. N. Kurdyumov, J.-C. Legros, H. Linde, V. I. Nekorkin, A. A. Nepomnyashchy, A. Ye. Rednikov, Yu. S. Ryazantsev, M. Santiago-Rosanne, P. Weidman and A. Wierschem. The research was supported by DGICYT PB96-599 (Spain) and by EU Network ERBFMRX-CT96-0010.

G. K. Batchelor, *The Theory of Homogeneous Turbulence* (Cambridge University Press, Cambridge,1953).

H. Bénard, Les tourbillon céllulaires dans une nappe liquide. Première partie: description générale des phénomènes, *Rev. Gén. Sci. Pures Appl.* **11** (1900) 1261.

H. Bénard, Les tourbillon céllulaires dans une nappe liquide transportant de le chaleur par convection en règime permanent, *Ann. Chim. Phys.* **23** (1901) 62.

R. V. Birikh, Thermocapillary convection in horizontal layer of fluids, *J. Appl. Mech. Tech. Phys.* **7** (1966) 43.

J. Bragard, M. G. Velarde, Bénard convection flows, *J. Non-Equilib. Thermodyn.* **19** (1997) 95.

J. Bragard, M. G. Velarde, Bénard-Marangoni convection: Theoretical predictions about planforms anf their relative stability, *J. Fluid Mech.* **368** (1998) 165.

F. H. Busse, Non-linear properties of thermal convection, *Rep. Prog. Phys.* **41** (1978) 1929.

C. I. Christov, M. G. Velarde, Dissipative solitons, *Physica D* **86** (1995) 323.

X.-L. Chu, M. G. Velarde, Korteweg-de Vries soliton excitation in Bénard-Marangoni convection, *Phys. Rev. A* **43** (1991) 1094.

X.-L. Chu, M. G. Velarde, Sustained transverse and longitudinal waves at the open surface of a liquid, *Physico Chem. Hydrodyn.* **10** (1988) 727.

R. Courant, K. O. Friedrichs, *Supersonic flow and shock waves* (Interscience Pub., N.Y., 1948).

S. H. Davis, Thermocapillary instabilities, *Ann. Rev. Fluid Mech.* **19** (1987) 403.

T. Doi, J. N. Koster, Thermocapillary convection in two immiscible liquid layers with free interface, *Phys. Fluids* **A5** (1993) 1914.

Ph. Drazin, R. S. Johnson, *Solitons. An Introduction* (Cambridge University Press, Cambridge,1989).

D. A. Edwards, H. Brenner, D. T. Wasan, *Interfacial Transport Processes and Rheology* (Butterworth-Heineman, Boston,1991).

U. Frisch, *Turbulence* (Cambridge University Press, Cambridge, 1995).

P. L. García-Ybarra, M. G. Velarde, Oscillatory Marangoni- Bénard interfacial instability and capillary-gravity waves in single- and two-component liquid layers with or without Soret thermal diffusion, *Phys. Fluids* **30** (1987) 1649.

A. N. Garazo, M. G. Velarde, Dissipative Korteweg-de Vries description of Marangoni- énard convection, *Phys. Fluids* **A3** (1991) 2295.

G.-X. Huang, M. G. Velarde, V. N. Kurdyumov, Cylindrical solitary waves and their interaction in Bénard-Marangoni layers, *Phys. Rev. E.* **57** (1998) 5473.

E. L. Koschmieder, *Bénard Cells and Taylor Vortices* (Cambridge University Press, Cambridge,1993).

P. Krehl, M. van der Geest, The discovery of the Mach reflection effect and its demonstration in an auditorium , *Shock Waves* **1** (1991) 3.

H. Lamb, *Hydrodynamics* (Dover, N. Y., 1945).

B. G. Levich, *Physicochemical Hydrodynamics* (Prentice-Hall, Englewood Cliffs, N.J., 1965).

H. Linde, X.-L. Chu, M. G. Velarde, Oblique and head-on collisions of solitary waves in Marangoni-Bénard convection, *Phys. Fluids* **A5** (1993) 1068.

H. Linde, X.-L. Chu, M. G. Velarde, W. Waldhelm, Wall reflection of solitary waves in Marangoni-Bénard convection, *Phys. Fluids* **A5** (1993) 3162.

H. Linde, M. G. Velarde, A. Wierschem, W. Waldhelm, K. Loeschcke, A. Ye. Rednikov, Interfacial wave motions due to Marangoni instability. I. Traveling periodic wave trains in square and annular containers, *J. Colloid Interf. Sci.* **188** (1997) 16.

H. Linde, M. G. Velarde, W. Waldhelm, A. Wierchem, Interfacial wave motions due to Marangoni instability. III. Solitary waves and (Jperiodic) wave trains and their collisions and reflections leading to dynamic network patterns, *J. Colloid Interf. Sci.* (2000) (submitted).

J. Lucassen, Longitudinal capillary waves, *Trans. Faraday Soc* **64** (1968) 2221.

P. Manneville, *Dissipative Structures and Weak Turbulence* (Academic Press, N.Y., 1990).

J. M. Miles, Korteweg-de Vries equation modified by viscosity, *Phys. Fluids* **19** (1976) 1063.

J. W. Miles, Obliquely interacting solitary waves, *J. Fluid Mech.* **79** (1977) 157; Resonantly interacting solitary waves, *J. Fluid Mech.* **79** (1977) 171.

V. I. Nekorkin, M. G. Velarde, Solitary waves of a dissipative Korteweg-de Vries equation describing Marangoni-Bénard convection and other thermoconvective instabilities, *Int. J. Bif. Chaos* **4** (1994) 1135.

A. A. Nepomnyashchy, M. G. Velarde, A three-dimensional description of solitary waves and their interaction in Marangoni-Bénard layers, *Phys. Fluids* **6** (1994) 187.

Ch. Normand, Y. Pomeau, M.G. Velarde, Convective instability: a physisist's approach, *Rev. Mod. Phys.* **49** (1977) 581.

S. Ostrach, Low-gravity fluid flows, *Ann. Rev. Fluid Mech.* **14** (1982) 313.

J. R. A. Pearson, On convection cells induced by surface tension *J. Fluid Mech.* **4** (1958) 489.

R. Pérez-Cordón, M.G. Velarde, On the (non linear) foundations of Boussinesq approximation applicable to a thin layer of fluid, *J. Phys. (Paris)* **36** (1975) 591.

A. Ye. Rednikov, P. Colinet, M. G. Velarde, J. C. Legros, Two-layer Bénard-Marangoni instability and the limit of transverse and longitudinal waves, *Phys. Rev. E.* **57** (1998) 2872.

A. Ye. Rednikov, P. Colinet, M. G. Velarde, J. C. Legros, Rayleigh-Marangoni oscillatory iinstability in a horizontal liquid layer heated from above: coupling and mode-mixing of internal and surface dilational waves, *J. Fluid Mech.* 2000 (to appear).

A. Ye. Rednikov, M. G Velarde, Yu. S. Ryazantsev, A. A. Nepomnyashchy, V. N. Kurdyumov, Cnoidal wave trains and solitary waves in a dissipation-modified Korteweg-de Vries equation, *Acta Appl. Math.* **39** (1995) 457.

J. S. Russell, *The Wave of Translation in the oceans of water, air and ether* (Trübner & Co., London, 1885) (An Appendix reproduces Russell's celebrated *Report on Waves* made to the meeting of the British Association for the Advancement of Science in 1842).

M. Santiago-Rosanne, M. Vigners-Adler, M. G. Velarde, Dissolution of a drop on a liquid surface leading to surface waves and interfacial turbulence, *J. Colloid Interface Sci.* **191**

(1997) 65.

L.E. Scriven, C.V. Sterling, The Marangoni effects, *Nature* **187** (1960) 186.

L. E. Scriven, C. V. Sternling, On cellular convection driven by surface-tension gradients: Effects of mean surface tension and surface viscosity, *J. Fluid Mech.* **19** (1964) 321.

C. V. Sternling, L. E. Scriven, Interfacial turbulence: Hydrodynamic instability and the Marangoni effect, *A. I. Ch. E. Journal*, **5** (1959) 514.

M. G. Velarde, Ch. Normand, Convection, *Sci. Amer.* **243** (1980) 92.

M.G. Velarde, R. Pérez-Cordón, On the (non-linear) foundations of Boussinesq approximation applicable to a thin layer of fluid. II. Viscous dissipation and large cell gap effects, *J. Phys. (Paris)* **37** (1976) 176.

M. G. Velarde, X.-L. Chu, A. N. Garazo, Onset of possible solitons in surface-tension-driven convection, *Phys. Scripta* **T35** (1991) 71.

M. G. Velarde, V.I. Nekorkin, A. Maksimov, Further results on the evolution of solitary waves and their bound states of a dissipative Korteweg-de Vries equation, *Int. J. Bif. Chaos* **5** (1995) 831.

P. Weidman, H. Linde, M.G. Velarde, Evidence for solitary wave behavior in Marangoni-Bénard convection, *Phys. Fluids* **A4** (1992) 921.

A. Wierschem, M. G. Velarde, H. Linde, W. Waldhelm, Interfacial wave motions due to Marangoni instability. II. Three dimensional characteristics of surface waves, J. *Colloid Interf. Sci.* **212** (1999) 365.

N. J. Zabusky, M. D. Kruskal, Interaction of "solitons" in collisionless plasma and the recurrence of initial states, *Phys. Rev. Lett.* **15** (1965) 57.

A. Zebib, G. M. Homsy, and E. Meiburg, High Marangoni number convection in a square cavity, *Phys. Fluids* **28** (1985) 3467.

Committee 5
Non-linear Structures in Natural Science and Economics

Draft – February 1, 2000
For Conference Distribution Only

Patterns, Waves, and Solitons in Fluids

Manuel G. Velarde
Professor of Physics
Universidad Complutense
Instituto Pluridisciplinar
Madrid, Spain

The Twenty-second International Conference on the Unity of the Sciences
Seoul, Korea February 9-13, 2000